# Nanoscale

Accepted Manuscript


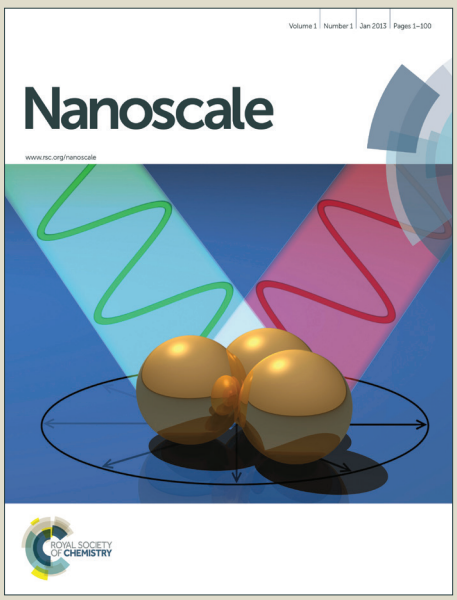





ROYAL SOCIETY OF CHEMISTRY

www.rsc.org/nanoscale

# Multi-functional liposomes having radiofrequency-triggered release and magnetic resonance imaging for tumor multi-mechanism therapy

Bin Du, Shuping Han, Hongyan Li, Feifei Zhao, Xiangjie Su, Xiaohui Cao and Zhenzhong Zhang*

Recently, nanoplatforms with multiple functions, such as tumor-targeting drug carrier, MRI, optical imaging, thermal therapy etc, have become popular in the field of cancer research. The present study devoted a novel multi-functional liposome for cancer theranostic. A dual targeted drug delivery with radiofrequency-triggered drug release and imaging based on magnetic field influence was used advantageously for tumor multi-mechanism therapy. In this system, iron oxide nanoparticles were decorated onto the surface of fullerene (C60), and PEGylation formed a hybrid nanosystem (C60-$Fe_3O_4$-$PEG_{2000}$). Thermosensitive liposomes (dipalmitoyl phosphatidylcholine, DPPC) with DSPE-$PEG_{2000}$-Folate wrapped up the hybrid nanosystem and docetaxel (DTX), which were designed to combine features of biological and physical (magnetic) drug targeting for fullerene radiofrequency-triggered drug release. The magnetic liposomes not only served as a powerful tumor diagnostic magnetic resonance imaging (MRI) contrast agent, but also as a powerful agent for photothermal ablation of tumor. Furthermore, a remarkable koinonia multi-functional liposome nanoplatform converted radiofrequency energy into thermal energy to release drug from thermosensitive liposomes, which was also observed during the treatment both in *vitro* and in *vivo*. The multi-functional liposomes also could selectively kill cancer cells in highly localized regions via

* *School of Pharmaceutical Sciences, Zhengzhou University, Science Road 100, 450001, Zhengzhou, China.E-mail address：zzzpaper@sina.com; Fax: + 86 371 67739546; Tel: + 86 371 67781910*

the excellent active tumor targeting and magnetic targeted abilities.

*Keywords*: Double-targeted; Magnetic liposomes; Radiofrequency-triggered; Imaging; Controlled release

## Introduction

Nanoscale liposomal formulations are one of the most advanced delivery systems for cytotoxic drugs. A liposome based DTX formulation has been approved for clinical use in cancer therapy and outperformed the free drug in therapeutic index. [1, 2] The therapeutic efficacy of liposomal formulations can be enhanced by receptor targeting and by stimuli-sensitive release within the tumor, like the decomposition of the formulation with increased temperature.[3] Hence, targeted and temperature-sensitive formulations attract much attention.

Folate receptor targeting has been found to be promising in liposomal drug delivery to cancers and has been demonstrated very effective in *vitro*. [4-6] However folate receptor targeted delivery could not increase drug concentrations in tumors when compared to a non-targeted stealth liposome formulation in *vivo*. [7, 8] Many cancer cells, including those implicated in cancers of the ovary, breast, brain, colon and lungs, tend to overexpress folic acid receptors. MCF-7 breast cancer cells have receptor-positive of folate and folic acid is able to transfect B16-F10 cells in the presence of higher concentration. It is true that folate receptor can high expression in MCF-7 breast cancer cells and B16-F10 cells.[9, 10] Magnetic nanoparticles are known for their immense potential in the fields of drug delivery, cancer diagnostics and therapeutics. [11-13] Magnetite nanoparticles (MNPs), in particular iron oxides, have been widely applied in biomedical fields due to low toxicity and good biocompatibility. [14] It is approved by Food and Drug Administration for in *vivo* usage and has been utilized in magnetic separation of

biological entities, thermal therapy and magnetic resonance imaging (MRI). [15-17] MNPs with high magnetization values and ultrafine particle sizes can be manipulated by external magnetic field by which human tissues can be penetrated, indicating the possibility of applying them for magnetic targeting. [15, 18] Among the broad spectrum of nanoscale materials being investigated for biomedical use, the MNPs have created significant interest due to their intrinsic magnetic properties for guided delivery of drugs and contrast agents for MRI.[19-21]

Magnetic liposomes (magnetic nanoparticles encapsulated within liposomes) appear to be a versatile delivery system due to biocompatibility, chemical functionality and their potential for a combination of drug delivery and radiofrequency thermal therapy of cancers. [22-24] Magnetic nanoparticles are used as drug carriers which accumulated in a target tissue, such as a tumor by a strong permanent gradient magnetic field. [25-27] Magnetic liposomes can also be used as T2 (spin–spin relaxation) contrast agent for MRI and thus their biodistribution can be monitored in *vivo* non-invasively by MRI. [28] For this purpose, iron oxide nanoparticles are injected directly into the tumor and exposed to an alternating magnetic field. [29-31]

Radiofrequency (RF) thermal therapy (RTT) uses RF absorbing agents to convert RF irradiation energy into heat, leading to the thermal ablation of cancer cells. In recent years, RTT has drawn widespread attention as a minimally invasive, controllable, and highly efficient treatment method. [32] The ability of RF radiation to penetrate into tissues with minimal energy loss has made RF activation system as a promising therapeutic strategy. Given the unique electrical and chemical properties of C60, [33-35] in this study, we hypothesized that exposure to a focused external RF field (13.56 MHz) would lead to significant heat release by the functionalized C60, allowing them to serve directly as an anticancer therapeutic agent. Further, the formulation would be temperature sensitive and allow the

release of chemotherapeutic drugs triggered by heat generated by fullerene under 13.56MHz RF.[36, 37] The fundamental requirement for receptor-mediated endocytosis into tumor cells in *vivo* is that the formulation extravagate from the blood circulation into the tumor tissue. Hence we follow the approaches and rely on shielded liposomal formulations that have been described to be long circulating and to extravasate based on the enhanced permeability and retention (EPR) effect. The latter is sufficient to warrant the retention of the formulation in the tumor. Gradient magnetic field targeting would support and accelerate these steps. Possibly, gradient magnetic field targeting would also enhance receptor-mediated uptake into tumor cells and thus also enhance the final step, tumor cell killing via radiofrequency triggered intracellular drug release.

At present, the technique of applying different individual functions into the cancer diagnosis and treatment is prevalent and mature. In order to integrate various functions into a single nanosystem for facilitating the treatment process, we try to make thermosensitive liposomes containing fullerene and magnetic iron oxide nanoparticle. Our goal in this study is to develop a nanoplatform with multifunctional characteristics for control release, dual-targeted drug delivery and imaging. These applications are complimentary to each other and provide the unique ability to serve as a cancer theranostic agent.

In this study, a C60-$Fe_3O_4$ nanocomposite was synthesized and then functionalized by polyethylene glycol ($PEG_{2000}$), giving C60-$Fe_3O_4$ with excellent stability in physiological solutions, and then folate receptor targeted thermosensitive liposomes wrapped up the hybrid nanosystems and DTX. The optimized liposome formulation consists of DPPC: cholesterol (Chol) : DSPE-PEG2000-Folate : DTX at 80:20:5:4 molar ratio. Herein, a tumor targeting liposome with multi-functional characteristics for RTT, control release and MRI applications (Fig.1) was developed and characterized by transmission

electron microscopy (TEM) and dynamic laser scattering (DLS). The RTT and tumor targeting efficacy of the nanosystem were examined using tumor cells and tumor-bearing mice models. Furthermore, in *vivo* MRI imaging of tumor-bearing mice using the multi-functional liposomes is also realized. The nanosystem developed in this work will be a promising multi-functional liposomes for cancer theranostic applications.

## Materials and methods

### Materials

All phospholipids were purchased from Avanti Polar Lipids Inc. (Alabaster, AL). Fullerene (C60, purity>95%) were purchased from Henan Fengyuan Chemicals Co. Ltd. DTX (purity>98%) was gotten from Beijing Yi-He Biotech Co. Ltd. Diethyl bromomalonate, NaH, $NH_2$-$PEG_{2000}$-$NH_2$, $FeCl_3 \cdot 6H_2O$, sodium acetate (NaOAc), ethylene glycol (EG), diethylene glycol (DEG), N-(3-dimethylamino propyl-N'-ethylcarbodiimide) hydrochloride (EDC·HCl), sodium dodecyl sulfate (SDS), and dimethyl sulfoxide (DMSO) were obtained from Sigma-Aldrich Co. LLC. Sulforhodamine B (SRB), dulbecco's minimum essential medium (DMEM), penicillin, streptomycin, fetal bovine serum (FBS), and heparin sodium were bought from Gibco Invitrogen. Other reagents were acquired from China National Medicine Corporation Ltd. The dialysis bags (MWCO=8,000) were from Spectrum Laboratories Inc.

### Synthesis of C60-$Fe_3O_4$-$PEG_{2000}$

Diethyl bromomalonate (0.2 mL) dissolved in toluene (3 mL) was added drop-wise to a stirred anhydrous toluene solution (50 mL) containing C60 (50 mg) and NaH (0.3 g). After stirring at room temperature under $N_2$ for 5 h, the mixture was concentrated to obtain malonate derivative of C60.

Malonate derivative of C60 (50 mg) and NaH (180 mg) were added to anhydrous toluene (30 mL), and stirred at 80℃ under $N_2$ for 10 h, then the concentrated HCl (20 mL) was added to the reaction precipitate, followed by removing toluene. The precipitate was dispersed in concentrated HCl, filtered and washed with $H_2O$ and MeOH. The resulting solid was dissolved in MeOH and the insoluble products were removed by filtering. After evaporation, the solid products were dried in vacuum at 50℃ for 24 h.[38]

In total, C60-COOH (50 mg), $FeCl_3 \cdot 6H_2O$ (270 mg), and sodium acetate (NaOAc,750 mg) were dissolved in a mixture of ethylene glycol (EG, 0.5 mL) and diethylene glycol (DEG, 9.5 mL). The resulting solution was then transferred to a teflon-lined stainless-steel autoclave, which was sealed and heated at 200℃ for 10 h. The as-prepared C60-$Fe_3O_4$ was washed several times with ethanol and deionized water, and dried in vacuum for 12 h.

Finally, 50 mg of $NH_2$-$PEG_{2000}$-$NH_2$ was added to a solution of C60-$Fe_3O_4$ (2 mg/mL, 10 mL) and ultrasonicated for 10 min. 5 mg of EDC·HCl was added to the solution. The reaction solution was stirred overnight at room temperature. The resulting product (C60-$Fe_3O_4$-$PEG_{2000}$) was purified by washing three times with deionized water through a membrane filter to remove unreacted PEG and other reagents, and dried in vacuum for 12 h.

**DTX adsorption on C60-$Fe_3O_4$-$PEG_{2000}$**

C60-$Fe_3O_4$-$PEG_{2000}$ (50 mg) was added to ethanol-water mixture (ethanol : water = 1:1, 50 mL) containing DTX (150 mg) and sonicated at room temperature for 2 h. After evaporation to remove ethanol and water, the product was dispersed in water (20 mL), and sonicated using an ultrasonic cell disruption system (400 W, 10 times). Then the nanosuspension was centrifuged to remove free DTX. The resulting C60-$Fe_3O_4$-$PEG_{2000}$/ DTX nanosuspension was stored at 4 ℃ until use.

**Preparation of DTX-loaded liposomes**

The liposomes within DPPC : Chol : DSPE-$PEG_{2000}$-Folate : DTX (molar ratio 80:20:5:4) were prepared by the thin film dispersion method, followed by sonography and membrane extrusion for size control. For preparing magnetic DTX-loaded liposomes, 20 mg of total lipid (DPPC : Chol : DSPE-PEG2000-Folate : DTX=80:20:5:4, containing 5 mg DTX) was dissolved in chloroform/diethyl ether (2/1, v/v) in a round bottom flask and the organic solvent was evaporated using a rotary evaporator at 60℃. The solvent was evaporated using a rotary evaporator to form a thin layer of lipid in the round bottom flask. Then, 1mg C60-$Fe_3O_4$-$PEG_{2000}$ powder was dissolved in 1 mL phosphate buffer (100 mM, pH 7.4). The lipid thin film was hydrated in this suspension at 60℃ for 20 min while rotating at 120 rpm at atmospheric pressure on a rotary evaporator. The resulting preparation was sonicated for 10 min and extruded through 400 nm, 200 nm and then 100 nm polycarbonate membranes using an extruder (Avanti Polar Lipids, USA) to adjust liposome size. Subsequently, the preparation was placed in millipore via centrifugation (Slide-A-Lyzer 10 kDa MWCO, Pierce Biotechnology, Rockford, IL, USA) at 12, 000 *g* for 30 min, un-encapsulated DTX was removed through the filtration membrane. The filtered liposomes were added 1% triton X-100 to make the liposomal membrane rupture. Then, the product was diluted with anhydrous ethanol and sonicated to ensure that DTX was dissolved completely, and centrifuged to separate C60-$Fe_3O_4$-$PEG_{2000}$ and DTX. The concentrations of DTX were determined by high performance liquid chromatography (HPLC, 1100 Agilent, USA) with the following conditions: an Eclipse XDB-C18 column (150 mm×4.6 mm, 5 μm); mobile phase methyl alcohol/water (75:25, v/v); column temperature 30℃; detection wavelength 229 nm; flow rate 1.0 mL/min; injection volume 20 μL. The DTX encapsulation efficiency was calculated using the following formula:

$$EE\% = (W_{encapsulate} / W_{total}) \cdot 100\%$$

Where $W_{encapsulate}$ and $W_{total}$ represent the amount of DTX in liposomes and the total amount of DTX in the system, respectively.

**Characterization**

FT-IR spectra of C60-$Fe_3O_4$-$PEG_{2000}$ were recorded on a Nicolet iS10 spectrometer (Thermo, USA). The relative amount of PEG linked to C60-$Fe_3O_4$ was tested using a thermal gravimetric analysis (TGA 4000, PerkinElmer, USA) with the experimental conditions of scanning from 25℃ to 800℃ under nitrogen at a heating rate of 20℃/min. The phase-transition temperature of liposomes was performed using differential scanning calorimetry (DSC, PerkinElmer, USA) from 30℃ to 60℃ at 3℃/min heating rate. Dynamic light scattering (DLS, Zetasizer Nano ZS-90, Malvern, UK) and transmission electron microscope (TEM, Tecnai G2 20, FEI, USA) were used for characterizing particle size, zeta potential and morphology of the nanoparticles. A vibrating sample magnetometer (VSM) was used for characterizing the magnetic property. The in *vitro* and in *vivo* $T_2$-weighted MR images were conducted on a 3-T clinical MRI scanner (Siemens, Erlangen, Germany).

***In vitro* release of DTX from liposomes**

In *vitro* DTX release study was performed with a dialysis method. PBS (pH7.4) containing 0.5% SDS was used as the release media. DTX, C60-$Fe_3O_4$-$PEG_{2000}$/DTX and multi-functional liposome samples were placed into dialysis bags (MWCO =8000 Da), which were added into 50 mL release media, respectively. The release experiment was performed at 37.0 ± 0.5℃ and 42.0 ± 0.5℃ with a stirring rate of 150 rpm/min. 0.2 mL solution was drawn from the dialysis bags at various time points, being replaced by the same volume of fresh release media. The concentration of DTX released from

nanosystems into media was quantified using HPLC under the above chromatographic conditions.

**Cell culture**

MCF-7 human breast cancer cell line was obtained from Chinese Academy of Sciences Cell Bank (Catalog No. HYC3204). Cells were cultured in normal DMEM with 10% FBS and 1% penicillin/streptomycin in 5% $CO_2$ and 95% air at 37℃ in a humidified incubator.

***In vitro* RTT treatment**

RTT treatment was monitored by sulforhodamine B sodium salt (SRB). SRB is a pink anionic dye, soluble in water, can be specifically combined with basic amino acid of compositive protein in cells under acid condition. At 540 nm wavelength, its absorption value is in direct proportion to cell uptake. MCF-7 cells were seeded at a density of 5,000 cells per well in flat bottom 96-well plates and incubated overnight. Thereafter, C60-$Fe_3O_4$-$PEG_{2000}$/DTX and the multi-functional liposomes were added with 200 μL fresh media in the wells of the plates and then exposed to 13.56 MHz RF (300 W) for 20 min to investigate RF sensitivity. After incubation for 24, 48 and 72 h at 37℃ in the $CO_2$ incubator, SRB assay was performed to determine cell viability. The same procedure was used to the multi-functional liposomes without irradiation.

**Cellular uptake**

Fluorescein isothiocyanate (FITC) in DMSO (1 mg/mL, 0.1 mL) was added to 5 mL of C60-$Fe_3O_4$-$PEG_{2000}$ nanosuspension, and the mixture was then sonicated and protected from light. Excess FITC was removed by Sephadex G-25 column (Sigma-Aldrich Co. LLC, USA). MCF-7 cells were seeded at $2\times10^5$ cells per well on glass cover slips in 6-well plates. When cells reached 70% confluence, they were treated with C60-$Fe_3O_4$-$PEG_{2000}$/DTX and multi-functional liposomes for 0.5, 1,

2 and 4 h, respectively. At indicated time points, cell medium was removed and cells were washed three times with PBS followed by soaking for 15 minutes in 4% paraformaldehyde, then washed with deionized water. The cells were imaged by a Fluorescence Microscope (Zeiss LSM 510, Thornwood, NY, USA).

**Determination of intracellular reactive oxygen species**

Reactive oxygen species (ROS) generation inside cells was detected using DCFH-DA Reactive Oxygen Species Assay Kit. MCF-7 cells were seeded in confocal dishes at a density of $5\times10^4$ cells/dish. Following incubation with C60-$Fe_3O_4$-$PEG_{2000}$/DTX and multi-functional liposomes for 6, 8, 12 and 24 h, dichlorofluorescin diacetate (DCFH-DA) was loaded in the cells. After 30 min incubation, cells were washed twice with PBS followed by exposed to 13.56 MHz RF (300 w) for 20 min. After irradiation, the fluorescence images of treated cells were acquired using a Fluorescence Microscope.

**Cell cycle analysis (PI staining)**

MCF-7 cells were harvested, after being incubated with DTX, C60-$Fe_3O_4$-$PEG_{2000}$/DTX/13.56 MHz, multi-functional liposomes and multi-functional liposomes/13.56 MHz RF for 24 h, then washed with PBS and fixed with 1 mL of cold 70% ethanol at $1\times10^6$ cells/mL for 30 min at 4℃. After centrifugation, the supernatant was discarded. The cells were washed with PBS, centrifuged and treated with 10 μL ribonuclease (10 mg/mL) at room temperature for 5 min. Then 400 μL of propidium iodide (PI, 50 μg/mL) was added to the samples. The cell cycle distribution was measured after 30 min incubation using Flow Cytometry (Beckman Coulter, CA, USA).

**Cells apoptosis assay**

Apoptosis was monitored by an Annexin-V-Fluos Staining kit (Sigma-Aldrich Co. LLC, USA). MCF-7 cells were treated with DTX, multi-functional liposomes, C60-$Fe_3O_4$-$PEG_{2000}$/DTX/13.56 MHz and multi-functional liposomes/13.56 MHz RF for 24 h under 37℃. Free DTX group was used as control. Cells were harvested, washed three times with cold PBS and re-suspended in 500 μL binding buffer. After adjusting cell density to $1\times10^6$ cell/mL, 5 μL Annexin V-FITC and 5 μL PI were added and incubated with the cells for 15 min in the dark. Finally, the stained cells were analyzed by a Flow Cytometry.

**Xenograft tumor mouse model**

All animal experiments were performed under a protocol approved by Henan Laboratory Animal Center. The B16-F10 tumor models were generated by subcutaneous injection of $1\times10^6$ cells in 0.1 mL saline into the right shoulder of C57 female mice (18-20 g, Henan Laboratory Animal Center). The mice were used when the tumor volume reached 60-100 $mm^3$ (~5 days after tumor inoculation).

***In vivo* antitumor effect**

The mice were divided into seven groups (six mice per group), minimizing the differences of weights and tumor sizes in each group. 0.2 mL of saline group, DTX, multi-functional liposomes, multi-functional liposomes/13.56 MHz RF (300 W, 20 min), multi-functional liposomes/magnet, C60-$Fe_3O_4$-$PEG_{2000}$/DTX/magnet/13.56 MHz RF, or multi-functional liposomes/magnet/13.56 MHz RF (DTX dose: 5 mg/kg) were intravenous injected into mice via the tail vein every 2 days. The mice were observed daily for clinical symptoms and the tumor sizes were measured by a caliper every other day and calculated as the volume = (tumor length) × $(\text{tumor width})^2/2$. After treatment for 14 days, the mice were killed to collect heart, liver, spleen, lung, kidney, brain and tumor, and the collected

tissues were soaked in 10% formalin solution, embedded with paraffin, then were divided into 2 shares for H&E stain and apoptosis test. Morphological changes and the number of apoptotic cells were observed and counted by Leica TCS-SP5 confocal microscope with the supplied software (Leica Confocal Software Version 2.0).

**Pharmacokinetic study**

0.5 mL blood was drawn from eyes of tumor-free healthy C57 mice after treatment of C60-$Fe_3O_4$-$PEG_{2000}$/DTX and multi-functional liposomes or DTX (DTX dose: 5 mg/kg) for 0.083, 0.25, 0.5, 1, 2, 4, 8 and 12 h, then centrifuged, the supernatant (0.2 mL) was placed into 5 mL centrifuge tubes. Methyltert-butyl ether (2 mL) was added to the above tubes and centrifuged after mixing by vortex. The supernatant was taken and dried by airflow (40℃), then, ethanol (0.1 mL) was added to dissolve DTX, and DTX in blood samples were detected by HPLC under the above chromatographic conditions. The pharmacokinetic parameters were calculated using Kinetica 4.4.1 program (Thermo. Fisher Scientific Inc., MA, USA).

**Biodistribution study**

For distribution studies, the tumor-bearing mice were fasted for 12 h before treatment, but had access to water adlibitum. The control group and experimental groups were given DTX, C60-$Fe_3O_4$-$PEG_{2000}$/DTX/magnet, multi-functional liposomes and multi-functional liposomes/magnet, respectively (DTX dose: 5 mg/kg). In magnet group, a magnet was glued onto the tumor site of the mice. After treatment for 0.5, 1, 3, 6 and 12 h, tissues were collected, weighed, and homogenized in buffer (acetonitrile to saline ratio, 1:3). The DTX contents in the tissues were determined using the method described previously. DTX in tissues were determined by HPLC under the above

chromatographic conditions.

***In vivo* MR imaging**

For in *vivo* MR imaging, the tumor-bearing mice were intravenously injected with multi-functional liposomes (0.2 mL, 50 mg/kg), and sticked magnet in the tumor. The magnet was taken away before MRI. Saline group was used as control. After injection for 1, 4 and 7 h, MR imaging was conducted on a 3-T clinical MRI scanner (Magnetom Symphony, Siemens Medical solutions, Erlangen, Germany).

**Statistical analysis**

Quantitative data were expressed as the mean ± standard deviation. Means were compared using the Student's *t*-test with SPSS 17.0 statistical software (SPSS Inc, Chicago, IL, USA), and *P*-values< 0.05 were considered to be statistically significant.

# Results and discussions

**Synthesis and characterization of C60-$Fe_3O_4$-$PEG_{2000}$ and multi-functional liposomes**

The inherent hydrophobicity limits the use of C60. To overcome this obstacle, carboxyl (-COOH) was introduced to the surface of C60. C60-COOH was synthesized by bingle cycloaddition reaction and ester hydrolysis reaction according to the procedure of literature with minor modifications. C60 was water-insoluble (Fig.2 A, a), while C60-COOH was stable in water over multiple weeks without significant aggregation (Fig. 2 A, b), implying successful introduction of -COOH onto C60. The $Fe_3O_4$ decorated onto the surface of water-soluble C60 generated C60-$Fe_3O_4$, which was not soluble in water (Fig. 2 A, c), thus could not be used in biological systems. To improve the solubility and biocompatibility of C60-$Fe_3O_4$, PEGylation was performed via a condensation of carboxyl of C60-$Fe_3O_4$ and $NH_2$ group of $NH_2$-$PEG_{2000}$-$NH_2$. The resulting C60-$Fe_3O_4$-$PEG_{2000}$ exhibited

excellent stability in water (Fig.2 A, d).

The results of FT-IR also showed new peaks at C=O (~1712 $cm^{-1}$) and O-H (~3418 $cm^{-1}$) in the spectrum of C60-COOH (Fig. 2 B, b) compared with C60 (Fig. 2 B, a), suggesting that the functionalization of C60 with -COOH was successful.[39] The C60-$Fe_3O_4$ was synthesized by chemical deposition of iron oxide nanoparticles onto C60 through a hydro thermal reaction (Fig. 2 B, c). During this reaction, a part of carboxyl group in C60-COOH was reduced, so the FT-IR spectrum of C60-$Fe_3O_4$ showed an obvious decrease in C=O and O-H peaks.[40] And a new peak generate at Fe-O (~570 $cm^{-1}$) (Fig.2 B, c). The successful PEGylation of C60-$Fe_3O_4$-$PEG_{2000}$ was also evidenced by its FT-IR spectrum, in which strong C-H (~1140 $cm^{-1}$), amide I (~1657 $cm^{-1}$), amide II (~1600 $cm^{-1}$) vibration peaks were clearly seen (Fig. 2 B, d).

The relative amount of PEG grafted onto the surface of C60-$Fe_3O_4$ was tested by TGA. PEG degraded completely at about 500℃ (Fig. 2 C), C60-$Fe_3O_4$ and C60-$Fe_3O_4$-$PEG_{2000}$ showed about 5% and 37% weight losses at 500℃, respectively, thus the relative amount of PEG grafted onto C60-$Fe_3O_4$ was 32%.

The DSC thermogram of conventional liposomes showed the phase transition peak at 163.4℃, and multi-functional liposomes showed a lower transition temperature with the main phase transition peaks at 41.5℃ (Fig.2 D). The lower transition temperature observed with multi-functional liposomes is due to the presence of DPPC lysolipid in the lipid bilayer, which leads to a slightly less ordered phospholipid molecule arrangement in the gel phase.

We found that C60-$Fe_3O_4$-$PEG_{2000}$ tend to form monodisperse aggregates in the size range of 100~200 nm as confirmed by DLS and TEM. The size and zeta potential of C60-$Fe_3O_4$-$PEG_{2000}$/DTX were 163.8 ± 3.7 nm (Fig. 3 A) and -33.4 ± 2.3 mV (Fig. 3 B), respectively. The size and zeta potential

of multi-functional liposomes were 187.0 ± 4.2 nm (Fig. 3 C) and -33.6 ± 2.1 mV (Fig. 3 D), respectively. The morphology of C60-$Fe_3O_4$- $PEG_{2000}$/ DTX was characterized by TEM. As can be seen from TEM images, C60-$Fe_3O_4$-$PEG_{2000}$/ DTX had a ball-like structure (Fig. 3 E), while $Fe_3O_4$ was scattered in the vision, suggesting $Fe_3O_4$ was successfully deposited on C60-COOH. TEM images (Fig. 3 F) indicated that the multi-functional liposomes had a uniform size and a ball-like structure. Compared with C60-$Fe_3O_4$-$PEG_{2000}$, the size of the multi-functional liposomes were a little bigger, this is probably due to the longtime of ultrasonic dispersion in preparation of the multi-functional liposomes.

The multi-functional liposomes displayed strong magnetic property. The nanocomposites can act as a $T_2$ contrast agent for MR imaging. [41-43] $T_2$-weighted MR images of the multi-functional liposomes acquired on a 3-T MR scanner revealed the concentration dependent darkening effect. It can be easily seen that smaller concentration of the nanocomposites gives much brighter $T_2$-weighted images (Fig. 4 A). The transverse relaxivity ($R_2$) of the multi-functional liposomes was measured to be 117.29 mg $mL^{-1}s^{-1}$(Fig. 4B). The magnetization hysteresis loop further indicated the superpara-magnetic nature of the multi-functional liposomes (Fig. 4 C).

The multi-functional liposomes were prepared by optimizing conditions, and encapsulation efficiency of the optimal prescription reached 91%. In order to evaluate DTX release in *vitro*, we incubated the nanostructures in sodium dodecyl sulfate solution (SDS, 0.5%). At 37℃, DTX and C60-$Fe_3O_4$-$PEG_{2000}$/DTX reached released balance after 1 h and 8 h of incubation. Under the same conditions, the multi-functional liposomes showed higher stability since 10% and 60% of DTX were released after 30 min and 48 h, respectively, and was still released slowly (Fig. 5 A). After determination of the stability at 37℃, DTX leakage from the liposomes was studied at 42℃. The

multi-functional liposomes approximate 100% released of their DTX content at 42℃ within 30 min, while DPPC/C60-$Fe_3O_4$-$PEG_{2000}$ /DTX released 70% in the first 5 min of incubation and reached 100% after 25 min of incubation (Fig. 5 B). The above results show that we can control the release rate of thermosensitive liposomes by adjusting temperature.

**Inhibition efficiency on MCF-7 cells**

The cytotoxicity study of the multi-functional liposomes on MCF-7 cells was shown in Fig. 6. Under 13.56 MHz RF, the multi-functional liposomes had higher inhibition efficiency on MCF-7 cells than non-irradiation. Furthermore, obvious difference between C60-$Fe_3O_4$-$PEG_{2000}$/DTX and the multi-functional liposomes was found. This is probably due to that DSPE-$PEG_{2000}$-Folate as active targeting delivery system can be transferred into cells faster, [44] and as a result, its effects are significantly better than the other two groups. It was also found that the multi-functional liposomes had higher inhibition efficiency on MCF-7 cells than DTX at all the time points, suggesting that the delivery system could deliver more drugs into tumor cells and enhance efficiency of inhibition on MCF-7 cells.

**Enhanced cell uptake of DTX by MCF-7 cells**

To track C60-$Fe_3O_4$-$PEG_{2000}$ inside cells, C60-$Fe_3O_4$-$PEG_{2000}$ was labeled with FITC through π–π stacking of C60. Fluorescence microscopy was applied to track the location of fluorescent-labeled C60 inside cells (Fig. 7). Little FITC was observed inside MCF-7 cells treated with FITC alone, indicating that FITC itself cannot permeate MCF-7 cells. The results showed that the multi-functional liposomes delivery system could effectively enhance uptake of the multi-functional liposomes/FITC by MCF-7 cells and this uptake was time-dependent manners (Fig. 7). The uptake of the multi-functional

liposomes/FITC by MCF-7 cells was more than that of C60-$Fe_3O_4$-$PEG_{2000}$/DTX/FITC by MCF-7 cells. This distinction in uptake could be explained for the difference in susceptibility of three DTX formulations to MCF-7 cells.

**Generation of intracellular ROS**

The level of intracellular ROS was an important indicator for RTT. Therefore, intracellular ROS induced by C60-$Fe_3O_4$-$PEG_{2000}$/DTX and the multi-functional liposomes under the 13.56 MHz RF was also determined. ROS productions were observed in MCF-7 cells incubated with C60-$Fe_3O_4$-$PEG_{2000}$/DTX and the multi-functional liposomes by using DCFH-DA fluorescent probe (Fig. 8). As shown in Fig. 8, green fluorescence of DCFH was observed in cancer cells incubated with C60-$Fe_3O_4$-$PEG_{2000}$/DTX and the multi-functional liposomes for 6 h and then exposed to a 13.56 MHz (300 W) RF for 15, 20, 25, 30 min, whereas control cells or without laser irradiating showed negligible DCFH fluorescence. Green fluorescence of DCFH was observed for MCF-7 cells treated by the multi-functional liposomes after RF exposure, in comparison to those treated with the multi-functional liposomes without RF, indicated that the multi-functional liposomes greatly improved the RTT efficacy of DTX. However, no significant difference was found between C60-$Fe_3O_4$-$PEG_{2000}$/DTX and the multi-functional liposomes with RF exposure.

**DTX formulations arrest cell cycle progression**

In order to understand how DTX could regulate breast cancer cell growth, the MCF-7 cells were treated with DTX, the multi-functional liposomes, C60-$Fe_3O_4$-$PEG_{2000}$/DTX/13.56 MHz RF and the multi-functional liposomes/13.56 MHz RF for 24 h. Flow cytometric analysis (Fig. 9 A) showed significant decrease in the percentage of cells in G1/G0 to 20.36 ± 0.56% in the multi-functional

liposomes/13.56 MHz RF group, as compared to C60-$Fe_3O_4$-$PEG_{2000}$/DTX/13.56 MHz RF group (33.26 ± 0.87%) and the multi-functional liposomes without RF group (42.83 ± 0.37%), the ratio of G1/G0 had a obvious trend of decline. Compared with the control group, the amount of cells in G2/M and S phase was a trend of increase from 1.59 ± 0.56% to 24.41 ± 0.54% ($p$ <0.05) and from 31.26 ± 0.47% to 53.49 ± 0.87% ($p$ <0.05), respectively.

**MCF-7 cells apoptosis**

Annexin V-FITC/PI apoptosis detection kit was used to study the cell apoptosis induced by DTX-loaded magnetic liposomes. Fig. 9 B showed the percentage of apoptosis and necrotic cells treated with different DTX formulations. The numbers of MCF-7 cells in early-apoptotic stage were significantly increased by following treatment with C60-$Fe_3O_4$-$PEG_{2000}$/DTX/13.56 MHz RF (1.5%) and the multi-functional liposomes/13.56 MHz RF (6.0%) than DTX alone (0.4%) (DTX dose: 50 μg/mL). Meanwhile, the results indicated that 52.1%, 46.4% and 29.0% of cells were in late-apoptotic stage following treatment with the multi-functional liposomes/13.56 MHz RF, C60-$Fe_3O_4$-$PEG_{2000}$ /DTX/13.56 MHz RF or the multi-functional liposomes for 24 h, respectively. The multi-functional liposomes with RF induced significant stronger cell apoptosis effect. The cytotoxicity and apoptosis study of DTX formulations confirmed that RF could make the multi-functional liposomes remarkably improve the cellular internalization of drug delivery systems, release more therapeutic agents into the cytoplasm and achieve stronger inhibition effect in *vitro*.

**Tumor growth inhibition *in vivo***

The surface temperature of tumor region reached to 43℃-45℃ with RF (300 W, 20 min) in the experiment. This suggested that drug could be released from multi-functional liposomes. To

investigate in *vivo* therapeutic efficacy of the multi-functional liposomes with 13.56 MHz RF, we conducted comparative efficacy studies. The changes of relative tumor volume as a function of time were plotted in Fig. 10 A. After 14 days treatment, control group showed a relative tumor volume ($V/V_0$) of 11.87 ± 0.67, the values of C60-$Fe_3O_4$-$PEG_{2000}$/DTX/magnet/13.56 MHz RF, the multi-functional liposomes/magnet and the multi-functional liposomes/13.56 MHz RF groups were 2.26 ± 0.65, 4.32 ± 0.74 and 3.28 ± 0.37, respectively. Compared with other therapeutic groups, the tumor of mice treated with the multi-functional liposomes/magnet/13.56 MHz RF was obviously reduced. This is a successful application that C60 was used as a heat production by RTT to release thermosensitive liposomes and achieve in *vivo* tumor treatment efficacy.[45] Because of the magnetic targeting property of the multi-functional liposomes, when a magnet was glued to the top of the tumor, more multi-functional liposomes would go to the tumor site than non-magnetic group, so the RTT efficacy of the multi-functional liposomes with a magnet was higher than that of non-magnetic group (Fig.10 A).[19] The growth of tumor tissue was successfully suppressed by the multi-functional liposomes/magnet/13.56 MHz RF. This high therapeutic efficacy originates from the high DTX and C60 accumulation in tumor tissue. Allowing for high toxicity usually leads to weight loss, body weight of the mice for all groups were measured during the treatments, the body weight in all groups increased during the treatments (Fig. 10 B), implying that the toxicity of treatments were not obvious.

Histological analysis of tumor tissue in different treatment groups at day 14 post-treatment (Fig. 10 C) revealed that the tumor cells in the control group showed vigorous growth, a tight arrangement, a large body and intact shape. Although cell necrosis, lysis, and fragmentation occurred in the multi-functional liposomes/magnet/13.56 MHz RF groups, there was no obvious difference between other groups.

**Pharmacokinetics**

To investigate the pharmacokinetics of various drug complexes, blood samples of C57 mice after injection of the multi-functional liposomes, C60-$Fe_3O_4$-$PEG_{2000}$/DTX or DTX at different time were determined by HPLC. The pharmacokinetic parameters were calculated by the two-compartment model. The results showed the decrease of DTX was faster than the multi-functional liposomes and C60-$Fe_3O_4$-$PEG_{2000}$/DTX after administration (Fig.11 A). Compared to C60-$Fe_3O_4$-$PEG_{2000}$/DTX, the area under the curve (AUC) of the multi-functional liposomes (53.65 μg h/mL) was about two times greater than that of C60-$Fe_3O_4$-$PEG_{2000}$/DTX (24.98 μg h/mL). The elimination rate of the multi-functional liposomes and C60-$Fe_3O_4$-$PEG_{2000}$/DTX were 18.64 (L/h kg) and 40.04 (L/h kg), respectively (Table 1). The mean residence time (MRT) of the multi-functional liposomes (5.66 h) was nearly two times longer than that of C60- $Fe_3O_4$-$PEG_{2000}$/DTX (2.14 h), indicating that the multi-functional liposomes significantly increased the blood circulation time of drug in *vivo*.

**Biodistribution**

To understand tumor treatment efficacy of various DTX formulations (DTX, Multi-functional liposomes, C60-$Fe_3O_4$-$PEG_{2000}$/DTX/magnet and Multi-functional liposomes/magnet), the distribution of DTX in tumor and various main organs was investigated. It was observed that significant differences for distributions of DTX in the four formulations (Fig.11 B, C, D, E). Differences in distributions of DTX were the most obvious at 3 h after injection. Importantly, the multi-functional liposomes/magnet and C60-$Fe_3O_4$-$PEG_{2000}$/DTX/magnet showed much higher DTX uptake in tumor than DTX and the multi-functional liposomes ($P$<0.05). In the multi-functional liposome group, DTX level in tumor (3h) was higher than that in the multi-functional liposomes and

C60-$Fe_3O_4$-$PEG_{2000}$/DTX/magnet group by about 1.9-fold and 1.6-fold, respectively. The ability of higher drug delivery efficiency to tumor for the multi-functional liposomes /magnet was striking and directly responsible for the higher tumor suppression efficacy in RTT. This is probably due to that DSPE-$PEG_{2000}$-Folate as active targeting delivery system and magnetic targeting together can reduce the distribution of the multi-functional liposomes in other organs, and increase distribution in the tumor to achieve better treatment of cancer.

***In vivo* MRI**

The excellent biocompatibility and high in *vitro* MRI contrast performance of the multi-functional liposomes inspired us to pursue their applicability for in *vivo* trials. Female C57 mice bearing B16-F10 tumors were intravenously injected with the multi-functional liposomes (200 μL, 50 mg/kg) with a magnet glued onto the tumor for 1, 4 and 7 h and imaged by a 3-T clinical MR scanner. Saline group was used as control. An obvious darkening effect in the tumor was observed in $T_2$-weighted MR images for 4 h (Fig. 12). After injection of the multi-functional liposomes for 7 h, the signal intensities of tumor were reduced remarkably. The darkening of the MR images in mouse other organs was weaker than signal of tumor, proving that the magnetic targeting property of the multi-functional liposomes existed in *vivo*. Consequently, these results suggested that the multi-functional liposomes could act as a suitable negative ($T_2$) contrast agent in MRI applications.

## Conclusions

A temperature sensitive folate-targeted docetaxel-containing magnetic liposome has been developed for thermo-chemotherapy of cancer. The liposome consists of DPPC: Chol: DSPE-$PEG_{2000}$-Folate at 80:20:5 molar ratio. Both the magnetic nanoparticles and DTX were successfully encapsulated within

the liposomes with high encapsulation efficiency. The multi-functional liposomes showed temperature sensitivity, strong responsiveness to magnetic fields which made folate receptor-mediated uptake into tumor cells. Taken together, the multifunctional properties of the liposomes enabled improved tumor cell killing in comparison to non-magnetic folate-targeted liposomes. Moreover, RF, magnetic targeting and folate active targeting synergistically increased the cytotoxicity in MCF-7 cells. From an optimized formulation for targeted thermo-chemotherapy of cancers, we expect enhanced accumulation in tumor tissue by physical targeting using a permanent magnetic gradient field. This should lead to a reduction of side effects compared to free DTX. We expect to enhance cellular uptake into tumor cells by virtue of the synergistic effect of RTT, biological and magnetic targeting.

## Acknowledgments

The authors thank Dr. Jinjin Shi (School of Pharmacy, Zhengzhou University) for assessment and technical support. We also thank Dr. Nan Zhang for her language edits. And this work was financially supported by the National Natural Science Foundation of China (Grant No. 81302717) and Innovation Team Project of Zhengzhou City (Grant No. 121PCXTD521).

## Notes and references

1 M.R. Ranson, S. Cheeseman, S. White and Margison, *Crit. Rev. Oncol. Hematol.,* 2001, **37**, 115–120.

2 J. Stebbing and A. Gaya, Cancer Treat. Rev., 2012, **28**,121–125.

3 T.L. Andresen, S.S. Jensen and K. Jorgensen, *Prog. Lipid. Res.,* 2005, **44**, 68–97.

4 S. Gorle, M. Ariatti and M. Singh, *Eur. J. Pharm. Sci.*, 2014, **59**, 83–93.

5 W. Gao, B. Xiang and T.T. Meng, *Biomaterials*, 2013, **34**, 4137–4149.

6 M.J. Turk, D.J. Waters and P.S. Low, *Cancer Lett.,* 2004, **213**,165–172.

7 J. Wu, Q. Liu and R.J. Lee, *Int. J. Pharm.,* 2006, **316**, 148–153.

8 A. Gabizon, H. Shmeeda, A.T. Horowitz and S. Zalipsky, *Adv. Drug Deliv. Rev.*, 2004, 56, 1177–1192.

9 J. Pan and S.S. Feng, *Biomaterials*, 2009, **30**, 1176–1183.

10 K. Urbiola, L. García, S. Zalba, M. J. Garrido and C.T. de Ilarduya, *Eur. J. Pharm. Biopharm.*, 2013, **83**, 358–363.

11 A.M . Shinkai, H. Honda and T. Kobayashi, *J. Biosci. Bioeng.*, 2005, **100**, 1–11.

12 S. Mornet, S. Vasseur, F. Grasset, P. Veverka, G. Goglio and A. Demourgues, *Prog. Solid State Chem.,* 2006, **34**, 237–247.

13 T. Neuberger, B. Schöpf, H. Hofmann, M. Hofmann and B. Rechenberg, *J. Magn. Magn. Mater.*, 2005, **293**, 483–496.

14 A.K. Gupta and M. Gupta, *Biomaterials* 2005, **26**, 3995–4021.

15 K.F. Ni, J.B. Yang, Y.H. Ren and D.Z. Wei. *Mater. Lett.,* 2014*,* **128***,* 392–395.

16 J. Riegler, J.A. Wells, P.G. Kyrtatos, A.N. Price, Q.A. Pankhurst and M.F. Lythgoe, *Biomaterials*

2010, **31**, 5366–5371.

17 K.Y. Choi, G. Liu, S. Lee and X.-Y. Chen, *Nanoscale*, 2012, **4**, 330 – 34.

18 V.I. Shubayev, T.R. Pisanic and S.Jin, *Adv. Drug Deliv. Rev.*, 2009, **61**, 467–484.

19 F. Dilnawaz, A. Singh, C. Mohanty and S.K. Sahoo, *Biomaterials,* 2010, **31**, 3694–3706.

20 G.N.Wang, X.J. Zhang, A. Skallberg, Y.X. Liu, Z.J. Hu, X.F. Mei and K. Uvdal, *Nanoscale*, 2014, **6**, 2953–2963.

21 B. Thierry, P. Kujawa, C. Tkaczyk, F.M. Winnik, L. Bilodeau and M. Tabrizian, *J. Am. Chem. Soc*., 2005, **127**, 1626–1627.

22 X. Fan, K.J. Nose, D.F. Diao and T. Yoshida, *Appl. Surf. Sci.*, 2013, **273**, 816–823.

23 A.A. Arie and J.K. Lee, *Synth. Met*., 2011, **161**,158–165.

24 T.T. Dao, T. Matsushima and H. Murata, *Org. Electron.*, 2012, **13**, 2709–2715.

25 S. Dandamudi, R.B. Campbell, *Biomaterials*, 2007, **28**, 4673–4683.

26 L. Zhang, W.F. Dong and H.B. Sun, *Nanoscale*, 2013, **5**, 7664–7684.

27 V. Plassat, M.S. Martina, G. Barratt, C. Menager and S. Lesieur, *Int. J. Pharm.*, 2007, **344**, 118–127.

28 M.S. Martina, J.P. Fortin, C. Menager, O. Clement, G. Barratt, C. Grabielle-Madelmont, F. Gazeau, V. Cabuil and S. Lesieur, *J. Am. Chem. Soc.*, 2005, **127**, 10676–10685.

29 S. Shen, F.F Kong, X.M Guo, L. Wu, H.J. Shen, M. Xie, X.S. Wang, Y. Jin and Y.R. Ge, *Nanoscale*, 2013, **5**, 8056–8066.

30 G.M. Huang, J. Hu, H. Zhang, Z.J. Zhou, X.Q Chi and J.H. Gao, *Nanoscale*, 2014, **6**, 726–730.

31 U. Schillinger, T. Brill, C. Rudolph, S. Huth, S. Gersting, F. Krötz, J. Hirschberger, C. Bergemann and C. Plank, *J. Magn. Magn. Mater.*, 2013, **239**, 501–508.

32 P. Cherukuri, E.S. Glazer and S.A. Curley, *Adv. Drug Deliv. Rev.*, 2010, **62**, 339–345.

33 S.A. Curley, P. Cherukuri, K. Briggs, C.R. Patra, M. Upton, E. Dolson and P. Mukherjee, *J. Exp. Ther. Oncol.*, 2008, **7**, 313–326.

34 C.J. Gannon, P. Cherukuri, B.I. Yakobson, L. Cognet, J.S. Kanzius, C. Kittrell, R.B. Weisman, M. Pasquali, H.K. Schmidt, R.E. Smalley and S.A. Curley, *Cancer*, 2007, **110**, 2654–2665.

35 G.L. Pakhomov, M.N. Drozdov, V.V. Travkin, M.A. Lopatin and V.I. Shashkin, *Synth. Met.,* 2014, **195**, 91–96.

36 K. Nowak, A. Krokosz, A. Rodacka and M. Puchala, *Radiat. Phys. Chem.*, 2014, **97**, 325–331.

37 J.U.Ahamed and R. Hatakeyama, *Mater. Sci. Eng. B*, 2012, **177**, 1660–1663.

38 J.J. Shi, L.Wang, J. Gao, Y. Liu, J. Zhang, R. Ma, R.Y. Liu and Z.Z. Zhang, *Biomaterials,* 2014,**35**,5771–5784.

39 J.J. Shi, Z. Wang, L. Wang, H. Wang, L. Li, X. Yu, J. Zhang, R. Ma and Z.Z. Zhang, *Int. J. Nanomedicine*, 2013, **8**,1551–1562.

40 H.M. Sun, L.Y. Cao and L.H. Lu, *Nano. Res.*, 2011, **4**, 550–562.

41 X. Shi, H. Gong, Y. Li, C. Wang, L. Cheng and Z. Liu, *Biomaterials,* 2013, **34**, 4786–4793.

42 O.M. Girard, R. Ramirez, S. McCarty and R.F. Mattrey, *Contrast Media Mol. Imaging*, 2012, **7**, 411–417.

43 M.M. Selvi, P. Manimuthu, K.S. Kumar and C. Venkateswaran, *J. Magn. Magn. Mater.*, 2014, **369**,155–161.

44 S. Lee and N. Murthy, *Biochem. Biophys. Res. Commun.*, 2007, **360**, 275–279.

45 A.A. Elsherbini, M. Saber, M.Aggag, A. El-Shahawy and H.A. Shokier, *Int. J. Nanomedicine*, 2011, **6**, 2155–2165.